Available online at www.sciencedirect.com
SCIENCE DIRECT®
Journal of Molecular and Cellular Cardiology xx (2006) xxx–xxx
Journal of Molecular and Cellular Cardiology
www.elsevier.com/locate/yjmcc

Original article

Mechanism of the Frank–Starling law—A simulation study with a novel cardiac muscle contraction model that includes titin and troponin I

Natalie S. Schneider [a,*], Takao Shimayoshi [b], Akira Amano [c], Tetsuya Matsuda [c]

[a] *Cell/Biodynamics Simulation Project Kyoto University, Kyoto, Japan*
[b] *ASTEM Research Institute of Kyoto, Kyoto, Japan*
[c] *Department of Systems Science, Graduate School of Informatics, Kyoto University, Kyoto, Japan*

Received 4 April 2006; received in revised form 5 June 2006; accepted 7 June 2006

Abstract

A stretch-induced increase of active tension is one of the most important properties of the heart, known as the Frank–Starling law. Although a variation of myofilament Ca^{2+} sensitivity with sarcomere length (SL) change was found to be involved, the underlying molecular mechanisms are not fully clarified. Some recent experimental studies indicate that a reduction of the lattice spacing between thin and thick filaments, through the increase of passive tension caused by the sarcomeric protein titin with an increase in SL within the physiological range, promotes formation of force-generating crossbridges (Xbs). However, the mechanism by which the Xb concentration determines the degree of cooperativity for a given SL has so far evaded experimental elucidation. In this simulation study, a novel, rather simple molecular-based cardiac contraction model, appropriate for integration into a ventricular cell model, was designed, being the first model to introduce experimental data on titin-based radial tension to account for the SL-dependent modulation of the interfilament lattice spacing and to include a conformational change of troponin I (TnI). Simulation results for the isometric twitch contraction time course, the length-tension and the force–$[Ca^{2+}]$ relationships are comparable to experimental data. A complete potential Frank–Starling mechanism was analyzed by this simulation study. The SL-dependent modulation of the myosin binding rate through titin's passive tension determines the Xb concentration which then alters the degree of positive cooperativity affecting the rate of the TnI conformation change and causing the Hill coefficient to be SL-dependent.

Keywords: Biological-based model; Cardiac muscle contraction; Cooperativity; Frank–Starling law; Titin; Troponin I

1. Introduction

Stretching of the ventricles due to greater end-diastolic volume results in greater systolic contraction force. This fundamental law of the heart, known as the Frank–Starling law, mainly stems from myofilament Ca^{2+} sensitivity increasing with sarcomere length (SL) within the physiological range (1.7 to 2.2 μm for small rodents [1]), leading to increased active tension from greater initial SL. This characteristic, known as the length–tension relationship (LTR), was found to be steeper in cardiac muscle than in skeletal muscle [2,3]. Despite its importance, the complex mechanisms underlying the Frank–Starling law are not fully understood [4,5]. Recent experimental progress favored the lattice spacing theory over the idea of a length-sensing element in the sarcomere [6]. It was suggested that the giant sarcomeric protein titin [7], which exhibits passive tension, modulates the spacing between thin and thick filaments [8,9]. In contrast to the titin isoforms found in cardiac muscle, titin in skeletal muscle produces only weak passive tension within the physiological SL range [10]. In mammalian heart, two isoforms were detected: N2B titin exhibits a greater passive stiffness than N2BA titin. The N2BA/N2B ratio is highly species-dependent, and a change in the ratio was found in diseased hearts [7].

Abbreviations: LTR, length–tension relationship; Tn, troponin; TnC, troponin C; TnT, troponin T; TnI, troponin I; SL, sarcomere length; Xb, crossbridge; Tm, tropomyosin; n_H, Hill coefficient; EC_{50}, $[Ca^{2+}]$ at half maximum tension; TTP90, time to 90% of peak tension; R50, time to 50% relaxation measured from peak tension; RU, regulatory unit; FCaR, force–$[Ca^{2+}]$ relationship; A, actin; E, equation; PKA, protein kinase A; SR, sarcoplasmic reticulum; KM, Kyoto Model.

* Corresponding author. Tel.: +81 75 326 1367; fax: +81 75 315 3198.
E-mail address: nati@biosim.med.kyoto-u.ac.jp (N.S. Schneider).

0022-2828/$ - see front matter © 2006 Elsevier Inc. All rights reserved.
doi:10.1016/j.yjmcc.2006.06.003

It is now believed that titin's passive tension, which rises with an increase of the SL within the physiological range, diminishes the interfilament space and accelerates force-generating, i.e. strong, crossbridge (Xb) formation [5]. However, the mechanism by which titin-based passive tension may change cooperative activation of the thin filament is far less well understood. It might result from the reduced lattice spacing which leads to an increase of Xbs [9]. Several experiments gave evidence for a role of the Xb concentration in the modulation of Ca^{2+} sensitivity [6]. An increase in Ca^{2+} sensitivity at shorter SLs was achieved by adding NEM-S1, a modified myosin head that produces strong nonforce generating Xbs [11], or MgADP, which diminishes the rate of Xb detachment and thus enhances the population of strong Xbs [12], or by reducing the MgATP concentration from 5 to 0.5 mM, which also increases the number of strong Xbs [13]. Alternatively, a decrease in the number of strong Xbs which was attained by lowering the pH (i.e. acidosis) or by addition of inorganic phosphate, resulted in a greater variation of active tension in response to SL changes [14]. These data clearly show that the concentration of Xbs is capable of modulating Ca^{2+} sensitivity. However, the underlying mechanism has not been elucidated. Recently, a biochemical in vitro study with purified labeled proteins showed that the conformational change of TnI consisting of two steps, binding of the TnI regulatory region to hydrophobic sites in the N-domain of Ca^{2+}-bound TnC and release of the adjacent TnI inhibitory region from actin, is an important regulatory switch in the Ca^{2+} activation of thin filaments [15]. The same study found that both Ca^{2+} and strong Xbs are required for full-strength activation of myofilaments.

To our knowledge, no simulation study to reveal potential Frank–Starling mechanisms was carried out. This may be due to the fact that existing myocyte contraction models are not suitable for such a study, since they include lumped states and lack titin. Here we report a new kind of cardiac muscle contraction model that includes titin and the conformational change of TnI. Analysis of this model revealed a working hypothesis for a Frank–Starling mechanism linking lattice space changes through titin-based passive tension with a change in cooperativity. Furthermore, the model well reproduces important isometric muscle contraction characteristics and seems to explain the SL dependency of the Hill coefficient (n_H). A preliminary study was published as a conference report [16].

2. Methods

2.1. Model structure

Actin filaments are composed of regulatory units (RU) with one RU consisting of seven actin (A) molecules, one troponin (Tn) complex (TnC, TnI, TnT) and one tropomyosin (Tm) molecule. Ca^{2+} binding to TnC is followed by a conformational change of TnI and Tm to clear the myosin binding site on actin [17]. This newly developed cardiac muscle contraction model combines Ca^{2+} activation and acto-myosin kinetics with a structure based on these molecular findings of myofilament activation. The model is given by a seven-state system of RUs, each in a different activation state and/or conformation (Fig. 1). First, Ca^{2+} binds to TnC of a not-activated RU (RUNA) to yield RUTCaoff, a state with Ca^{2+} bound to TnC but with TnI still bound to actin. Then a conformational change releases TnI from its inhibitory region on actin (RUTCaon). This step was shown to be an important regulatory switch [15]. The subsequent conformational change of Tm creates fully activated RUs (RUTMon) with a free myosin binding site. Myosin with a technically hydrolyzed ATP bound (MADPPi), a species mainly found at rest in a rapid equilibrium with MATP [18], can bind to RUTMon to form a nonforce-generating, i.e. weak, Xb (RUAMADPPi). In this state, the myosin binding pocket for P_i is closed. The subsequent force generation step results in an open P_i pocket and a strong Xb (RUA_MADPPi). P_i can then be released from the acto-myosin complex to yield a second strong Xb state (RUA_MADP) and finally ADP is released and the RUTMon state is recovered. The acto-myosin interactions described here are based on experimental findings [19] showing that P_i is released after the power stroke.

Three rate parameters, in particular k_{offI}, k_{tmon} and k_3 (Fig. 1), are subject to change due to cooperativity in filament activation. Cooperativity mechanisms are fundamental to cardiac muscle activation, since cardiac TnC exhibits only one Ca^{2+} specific binding site responsible for regulation of contraction, in

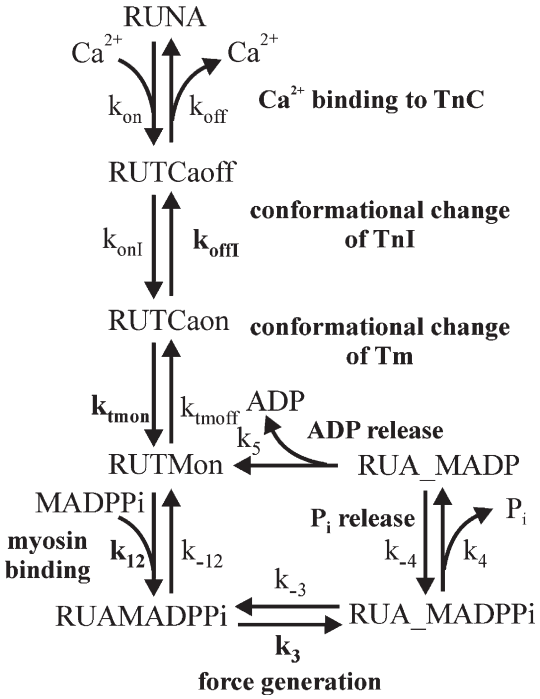

Fig. 1. State diagram for the cardiac contraction model (M1). The model consists of seven different states of an RU (RUNA: not activated RU; RUTCaoff: Ca^{2+} bound to TnC with TnI still bound to A; RUTCaon: TnI released from A; RUTMon: Tm in the activated conformation; RUAMADPPi: M with a hydrolyzed ATP bound to A of a activated RU=weak Xb; M pocket for P_i closed; RUA_MADPPi: strong Xb, M pocket for P_i open; RUA_MADP: strong Xb, P_i released from the acto-myosin complex). Bold rate parameters are dynamic with k_{offI}, k_{tmon} and k_3 changing due to cooperativity and k_{12} depending on titin-based radial force.

contrast to the two sites found in skeletal TnC [20]. Some positive and negative cooperativity mechanisms as analyzed by Robinson et al. [21] were employed, modified and adapted for the seven-state model. The myosin binding rate parameter (k_{12}) depends on titin-based radial force. Details on cooperativity and titin are outlined in Section 2.2. In this study, it was assumed that only one myosin head can be bound per RU [20].

The model was designed to be used in the Kyoto Model ventricular cell, a model that is based on guinea pig experimental data [22]. Due to a lack of guinea pig data for model adjustment, available data from other animals (mainly cat and mouse) were applied. The flexibility of the present model allows easy adjustment to data from human or other species. Presented here are results for isometric contractions only, i.e. constant SL, so this model description is restricted to chemical aspects.

2.2. Mathematical model

Each step of the seven-state model (Fig. 1), referred to as M1 in this paper, is explained in mathematical details below.

The sum of all RUs (RUTotal) is given by:

$$\begin{aligned}[\mathrm{RUtotal}] = {} & [\mathrm{RUNA}] + [\mathrm{RUTCaoff}] + [\mathrm{RUTCaon}] \\ & + [\mathrm{RUTMon}] + [\mathrm{RUAMADPPi}] \\ & + [\mathrm{RUA\_MADPPi}] + [\mathrm{RUA\_MADP}]. \end{aligned} \tag{1}$$

The net rate of Ca^{2+} binding to TnC (Q_{CaB}) is:

$$Q_{\mathrm{CaB}} = k_{\mathrm{on}} \cdot [\mathrm{RUNA}] \cdot [Ca^{2+}] - k_{\mathrm{off}} \cdot [\mathrm{RUTCaoff}] \tag{2}$$

where k_{on} and k_{off} are the binding and unbinding rate constants, respectively.

The net rate for the conformational change of TnI (Q_{TCaA}) is given by:

$$Q_{\mathrm{TCaA}} = k_{\mathrm{onI}} \cdot [\mathrm{RUTCaoff}] - k_{\mathrm{offI}} \cdot [\mathrm{RUTCaon}] \tag{3}$$

where k_{onI} is the rate for the change to the "on" conformation and k_{offI} for the "off" state. Unlike the Ca^{2+} binding step, the TnI change is subject to cooperativity expressed in a change of k_{offI} as follows:

$$\begin{aligned} k_{\mathrm{offI}} = {} & k_{\mathrm{offi}} \cdot \left[1 + k_{\mathrm{OFF}} \cdot \frac{[\mathrm{RUA}]}{[\mathrm{RUtotal}]}\right]^2 \\ & \times \left[1 + k_{\mathrm{xboff}} \cdot \frac{[\mathrm{RUA\_MADPPi}] + [\mathrm{RUA\_MADP}]}{[\mathrm{RUtotal}]}\right]^{4.4} \end{aligned} \tag{4}$$

with the activated RUs (RUA) given as:

$$\begin{aligned}[\mathrm{RUA}] = {} & [\mathrm{RUTCaon}] + [\mathrm{RUTMon}] + [\mathrm{RUAMADPPi}] \\ & + [\mathrm{RUA\_MADPPi}] + [\mathrm{RUA\_MADP}]. \end{aligned} \tag{5}$$

Both terms in E4 account for positive cooperativity, i.e. a decrease of k_{offI} during myofilament activation. The first term results from slowing down the back reaction if a neighboring RU is also in the activated conformation [21]. The second term accounts for the inhibition of the TnI actin re-association through strong Xbs [15]. Power 4.4 has been obtained through model fitting.

To fully activate myofilaments, a conformational change of Tm is necessary since it has to be moved away from the myosin binding site on actin which is the major structural change of the RU [20] leading to RUTMon. The net rate for this step (Q_{TMA}) is given as:

$$Q_{\mathrm{TMA}} = k_{\mathrm{tmon}} \cdot [\mathrm{RUTCaon}] - k_{\mathrm{tmoff}} \cdot [\mathrm{RUTMon}] \tag{6}$$

where k_{tmon} is the rate for the move of Tm away from the myosin binding site and k_{tmoff} the rate for the return to the nonactivated state. k_{tmon} is subject to change due to different cooperativity mechanisms.

$$\begin{aligned} k_{\mathrm{tmon}} = {} & k_{\mathrm{tmonc}} \cdot \left(\frac{[\mathrm{RUTCaon}]}{[\mathrm{RUtotal}]}\right) \cdot \left[1 + k_{\mathrm{tmRU}} \cdot \left(\frac{[\mathrm{RUTMon}]}{[\mathrm{RUtotal}]}\right)\right]^2 \\ & \times \left[1 + k_{\mathrm{tmxb}} \cdot \frac{([\mathrm{RUA\_MADPPi}] + [\mathrm{RUA\_MADP}])}{[\mathrm{RUtotal}]}\right]^2. \end{aligned} \tag{7}$$

The terms which include RUTCaon and RUTMon increase k_{tmon} during myofilament activation (positive cooperativity). The conformational change of the Tn complex may speed up the conformational change of Tm [15,17]. In addition, Tm molecules in the activated conformation may activate neighboring Tm molecules since all Tm molecules overlap in a head-to-tail configuration. This is expressed in the term containing RUTMon. Strong Xbs cause negative cooperativity which may be attributed to Xb-induced strain in Tm [21]. This has yet to be proofed.

The net rate of the myosin binding step (Q_{MB}) which leads to the formation of weak Xb is as follows:

$$\begin{aligned} Q_{\mathrm{MB}} = {} & k_{12} \cdot \mathrm{KTitin} \cdot [\mathrm{MADPPi}] \cdot [\mathrm{RUTMon}]_{\mathrm{eff}} \\ & - k_{-12} \cdot [\mathrm{RUAMADPPi}] \end{aligned} \tag{8}$$

where [MADPPi] is the concentration of myosin heads with technically hydrolyzed ATP bound, KTitin the titin function explained in details below, k_{12} is the myosin binding rate and k_{-12} the detachment rate. The concentration of activated RUs overlapping with the myosin filaments, $[\mathrm{RUTMon}]_{\mathrm{eff}}$, is SL-dependent:

$$[\mathrm{RUTMon}]_{\mathrm{eff}} = \alpha \cdot [\mathrm{RUTMon}] \tag{9}$$

α is the sarcomere overlap function that represents the fraction of thick filaments with myosin heads in single overlap conformation as described by Rice et al. [23]:

$$\begin{aligned} &\text{For } L < 1\ \mu\mathrm{m}: && \alpha = 1.5 \cdot \left(\frac{L}{L_0}\right) 0 - 0.5 \\ &\text{For } L \geq 1\ \mu\mathrm{m} \text{ and } L \leq 1.1\ \mu\mathrm{m}: && \alpha = 1 \\ &\text{For } L > 1.1\ \mu\mathrm{m}: && \alpha = -1.6 \cdot \left(\frac{L}{L_0}\right) + 2.76 \end{aligned} \tag{10}$$

where L is the half sarcomere length and L_0 a normalization factor.

The passive tension due to titin can be split into the longitudinal tension which results in compliance and the radial tension (F_{rad}) which modulates the lattice spacing between thick and thin filaments [8]. The titin isoform ratio (N2BA/N2B) depends on the heart rate with animals having a faster beating heart expressing mainly the stiffer N2B isoform [10,24]. Since only mouse skinned fiber experimental titin-based radial tension data [8] were available, they were modified as follows: (1) The F_{rad} data were shifted to smaller SL to account for the Ca^{2+} sensitivity difference of skinned vs. intact fibers [1]. (2) Since the guinea pig heart rate (230–300 beats/min) fits in between mouse (402–834 beats/min; ratio (N2BA/N2B): <0.05) and rabbit (205–220 beats/min; ratio: 0.2) [25] a higher ratio than that for the mouse, which correlates with a less steep F_{rad} curve was assumed (Fig. 2). The following equation which was obtained through a fit of the modified F_{rad} data was used to model the SL-dependent influence of titin on the lattice spacing:

$$f_{\text{titinNormal}} = \text{kTitin} \cdot \frac{9.9663}{1+e^{\frac{\left(\frac{L}{L_0}\right)+1.0639}{0.0696}}} \tag{11}$$

with kTitin being a scaling factor. A direct proportional relationship between titin F_{rad} and the change of the myosin binding speed was assumed in the model.

Stretching of cardiac muscle to above the maximum physiological SL which is around 2.2 μm for small rodents causes permanent damage of the passive tension [1]. Experimental data showed that this is probably a result of an irreversible unfolding of some of titin's Ig domains [26] which may lead to a progressive detachment of titin from the thick filament [27]. Hence, the lattice spacing should increase for higher SL.

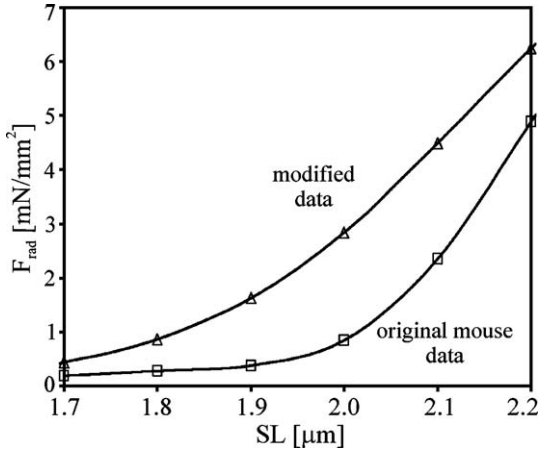

Fig. 2. Data for titin-based radial force. Original experimental data from mouse [1] used to fit $f_{\text{titinNormalM}}$ (E29) are compared to the modified data used to fit $f_{\text{titinNormal}}$ (E11).

To account for the titin damage a linear relationship with SL was assumed.

$$f_{\text{titinDamaged}} = \text{kTitin} \cdot \left(-31 \cdot \left(\frac{L}{L_0}\right) + 40\right). \tag{12}$$

The titin function (KTitin) consisting of the two different functions described above was defined as follows:

$$\text{KTitin} = \begin{cases} f_{\text{titinNormal}} & (L \leq 1.1\ \mu\text{m}) \\ f_{\text{titinDamaged}} & (L > 1.1\ \mu\text{m}) \end{cases}. \tag{13}$$

Since damaged elastic material shows different characteristics, the use of two discontinuous equations is justified. It was assumed that titin gets abruptly damaged at SL>2.2 μm although physiologically this is probably a smoother process best described by an intermediate function. However, in a normal functioning cardiac muscle passive tension prevents the muscle from overstretching, i.e. a SL>2.2 μm cannot be found, so titin damage is a rather nonphysiological process. Just to analyze if experimental findings of a steeper descending limb for the LTR in cardiac muscle might be caused by titin damage, $f_{\text{titinDamaged}}$ was added. Only for Fig. 4 a SL>2.2 μm was used for simulations.

The force generating step (Q_{Fgen}) is a fast conformational change of the actin bound myosin to open the P_i binding pocket associated with the formation of a strong Xb [19]. The following equation gives the net rate.

$$Q_{\text{Fgen}} = k_3 \cdot [\text{AMADPPi}] - k_{-3} \cdot [\text{AM\_ADPPi}] \tag{14}$$

where k_3 is the strong Xb formation and k_{-3} the detachment rate parameter. k_3 is subject to change due to cooperativity:

$$k_3 = k_{3c} \cdot \left[1 + k_{3f} \cdot \left(\frac{[\text{RUTCaon}]_{\text{eff}} + [\text{RUTMon}]_{\text{eff}} + [\text{RUAMADPPi}]}{[\text{RUtotal}]}\right)\right]^2 \times \left[1 + k_{3xb} \cdot \frac{([\text{RUA\_MADPPi}] + [\text{RUA\_MADP}])}{[\text{RUtotal}]}\right]^2 \tag{15}$$

with $[\text{RUTMon}]_{\text{eff}}$ given by E9 and

$$[\text{RUTCaon}]_{\text{eff}} = \alpha \cdot [\text{RUTCaon}]. \tag{16}$$

k_3 is enhanced through activated RUs (positive cooperativity). But strong Xbs slow down the reaction. This negative cooperativity may be due to strain and steric hindrance [21].

The P_i release is a reversible step with the net rate (Q_{PiR}) given as:

$$Q_{\text{PiR}} = k_4 \cdot [\text{RUA\_MADPPi}] - k_{-4} \cdot [\text{RUA\_MADP}] \tag{17}$$

with k_4 being the P_i release and k_{-4} the P_i attachment rate constants, respectively.

The ADP release is the rate limiting step of the isometric system and the backward reaction is negligible [19]. The net rate (Q_{ADPR}) is calculated as follows:

$$Q_{\text{ADPR}} = k_5 \cdot [\text{RUA\_MADP}]. \tag{18}$$

The rate changes for the different RU species and $[Ca^{2+}]$ are determined as follows:

$$\frac{d[RUTCaoff]}{dt} = Q_{CaB} - Q_{TCaA} \quad (19)$$

$$\frac{d[RUTCaon]}{dt} = Q_{TCaA} - Q_{TMA} \quad (20)$$

$$\frac{d[RUTMon]}{dt} = Q_{TMA} - Q_{MB} + Q_{ADPR} \quad (21)$$

$$\frac{d[RUAMADPPi]}{dt} = Q_{MB} - Q_{Fgen} \quad (22)$$

$$\frac{d[RUA\_MADPPi]}{dt} = Q_{Fgen} - Q_{PiR} \quad (23)$$

$$\frac{d[RUA\_MADP]}{dt} = Q_{PiR} - Q_{ADPR} \quad (24)$$

$$\frac{d[Ca^{2+}]}{dt} = -Q_{CaB}. \quad (25)$$

The active force F_b is proportional to the number of developed Xbs with A_{iso} being the force factor for isometric contractions [28].

$$F_b = A_{iso} \cdot ([RUA\_MADPPi] + [RUA\_MADP]). \quad (26)$$

Table 1 shows the parameter values used in all simulations unless indicated.

Table 1
Numerical values of parameters

Parameter	Value	Source
A_{iso}	9000 mN/mm^2/mM	[28]; (A*hc)
k_{off}	0.2/ms	[21]
k_{on}	17.3/mM/ms	[21]
[RUtotal]	0.0726 mM	Calculated for L_{max}=1.1 μm according to [20]
k_{onI}	0.2/ms	Model fit
k_{offi}	0.075/ms	Model fit
k_{OFF}	−0.32	Model fit
k_{xboff}	−1.37	Model fit
k_{tmoff}	0.067/ms	Model fit [44]
k_{tmonc}	0.014/ms	Model fit [44]
k_{tmRU}	10	Model fit
k_{tmxb}	−1.86	Model fit
L_0	0.001 mm	To normalize L
k_{12}	2/mM/ms	Model fit according to [57,58]
k_{-12}	0.6/ms	Model fit according to [57,58]
[MADPPi]	0.1375 mM	Calculated for L_{max}=1.1 μm according to [20]
kTitin	0.2	Model fit
k_{3c}	0.025/ms	Model fit according to [57]
k_{3f}	50	Model fit
k_{3xb}	−1.23	Model fit
k_{-3}	0.008/ms	Model fit according to [57]
k_4	0.077/ms	[19]
k_{-4}	0.001/ms	Model fit
k_5	0.03723/ms	[19]; T adjusted to 37 °C

2.3. Model variations

Modified models which have been used in this study are described below with the original model named M1. M2 lacks the titin function and uses E27 for the myosin binding step instead of E8.

$$Q_{MB} = k_{12} \cdot [MADPPi] \cdot [RUTMon]_{eff} - k_{-12} \cdot [RUAMADPPi]. \quad (27)$$

To test whether titin has a greater effect on the myosin binding rate or the force generating rate, in M3 the myosin binding step E8 has been exchanged to E27 and the titin function (KTitin, E13) added to the force generating step using E28 instead of E14.

$$Q_{Fgen} = k_3 \cdot KTitin \cdot [AMADPPi] - k_{-3} \cdot [AM\_ADPPi] \quad (28)$$

M4 employs a titin function fitted to the original mouse data [8]. For KTitin, E29 is used instead of E11 in the myosin binding step E8.

$$f_{titinNormalM} = kTitin \cdot \frac{9.5988}{1+e^{\frac{\left(-\frac{L}{L_0}+1.0997\right)}{0.0447}}} \quad (29)$$

In M5, the positive cooperativity caused by strong Xbs is omitted in k_{offI}. E30 is used instead of E4 with k_{OFF}=−0.5.

$$k_{offI} = k_{offi} \cdot \left[1 + k_{OFF} \cdot \frac{[RUA]}{[RUtotal]}\right]^2 \quad (30)$$

In M6, power 4.4 in E4 was changed to power 2. k_{xboff}=−2.3 is used to achieve a similar steep curve as with power 4.4. The model differences are summarized in Table 2.

2.4. Simulations and data analysis

The contraction model was implemented in Java using the *simBio* package [29], software for cell simulation. The differential equations were solved using an Euler method with dynamically adjusted time steps. Steady state simulations were carried out in an isolated model with constant $[Ca^{2+}]$, i.e. omitting E25 (Sections 3.2 and 3.3; Figs. 4 and 5). For the numerical analysis of species and rate parameter changes with $[Ca^{2+}]$, a separate Java program was used (Sections 3.1 and 3.4; Figs. 3 and 6). In those cases, the $[Ca^{2+}]$ was constant for each calculation point. To obtain a Ca^{2+} transient for isometric twitch contractions either the contraction model used in the Kyoto Model ventricular cell [22] was replaced by the present model (M1) (Section 3.5; Figs. 7A–D), or a module for a simple Ca^{2+} transient producing sarcoplasmic reticulum (SR) as described in [28]

Table 2
Differences of models used in this study

	Changed equations	Model description
M1	Original model	Titin effects myosin binding rate
M2	E8 changed to E27	No titin
M3	(1) E8 changed to E27 (2) E14 changed to E28	Titin effects force generating rate
M4	E11 changed to E29	Titin function fitted to the original mouse data
M5	E4 changed to E30 with $k_{OFF}=-0.5$	Xb caused cooperativity omitted in k_{offI}
M6	In E4 power 4.4 changed to power 2; $k_{xboff}=-2.3$	Validation of power 4.4

(E8 (Q_{pump}), E9 (Q_{rel}) from [28]) was added to M1, and E31 was used instead of E25 (Fig. 7E).

$$\frac{d[Ca^{2+}]}{dt} = Q_{rel} - Q_{pump} - Q_{CaB}. \quad (31)$$

The force–[Ca^{2+}] relationship (FCaR) for each SL was fitted to the Hill equation E32 by nonlinear regression analysis using SigmaPlot (Version 8.02; SPSS Inc.)

$$F = \frac{[Ca^{2+}]^n}{EC_{50}^n + [Ca^{2+}]^n} \quad (32)$$

where F is the normalized steady state force, EC_{50} is [Ca^{2+}] at which force is half-maximal, and n_H the slope of the FCaR (Hill coefficient).

3. Results

3.1. Numerical analysis of RU species and rate parameter changes with [Ca^{2+}]

Fig. 3 shows the numerical analysis of species concentrations and rate parameter changes during [Ca^{2+}] variation for M1 at two physiologically relevant SLs (2.2 μm (Figs. 3A, B) and 1.7 μm (Figs. 3C, D)). With addition of Ca^{2+} the concentration of RUs with Ca^{2+} bound to TnC (RUTCaoff) starts to rise initially. However, a sigmoidal decrease of k_{offI}, i.e. the prevention of TnI from returning to its inhibitory conformation, causes RUTCaoff to decrease with further increasing [Ca^{2+}] with a simultaneous sharp rise in RUTCaon (Fig. 1), which is the most abundant species at high [Ca^{2+}] at both SLs. The SL dependency of the k_{offI} decrease (Figs. 3B, D) is an important characteristic of M1, as explained in Section 3.4 below.

The concentration of fully activated RUs (RUTMon) increases as the SL decreases from 2.2 to 1.7 μm. This is

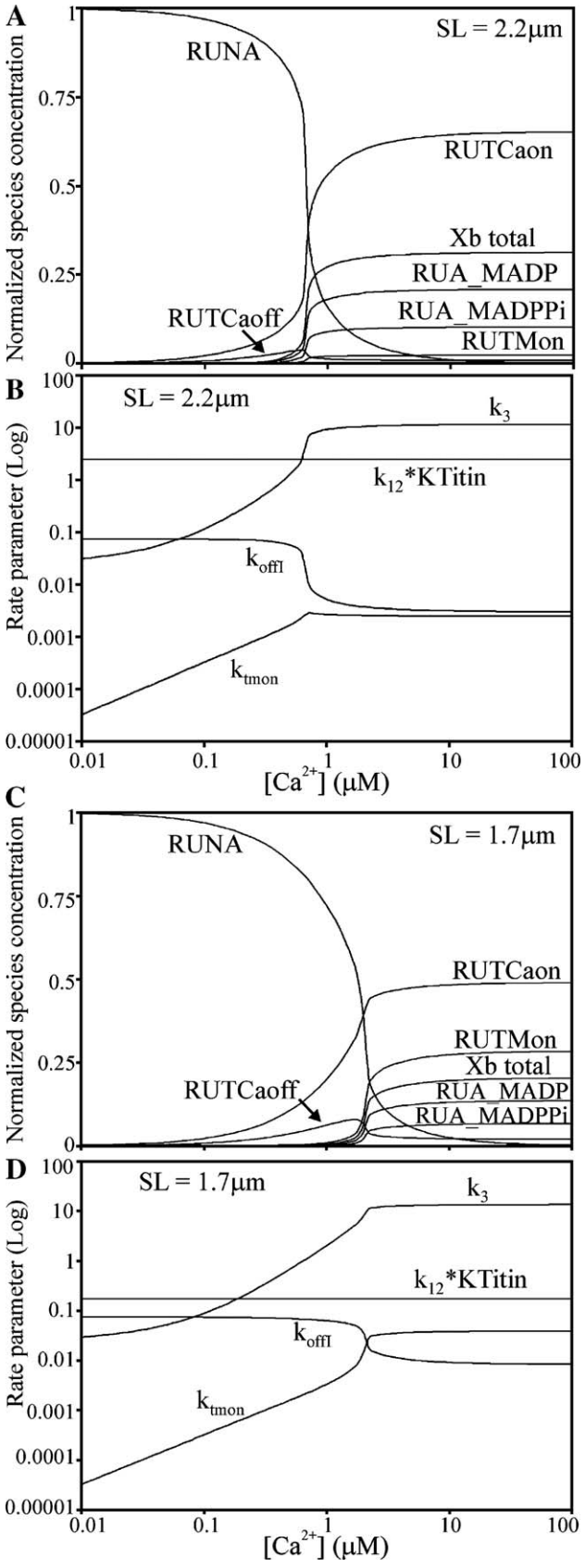

Fig. 3. Numerical analysis of RU species and rate parameter changes with [Ca^{2+}] for different SLs. Variation of state concentrations with [Ca^{2+}] at SL=2.2 μm (A) and SL=1.7 μm (C). [RUAMADPPi] is too small to be seen. Xb total gives the sum of strong Xbs ([RUA_MADPPi] and [RUA_MADP]). Rate variation (log_{10}) with [Ca^{2+}] for SL=2.2 μm (B) and SL=1.7 μm (D). The TnI (k_{off}) and Tm (k_{tmon}) conformational change rates and the force generation rate (k_3) vary with cooperativity. The myosin binding rate (k_{12}*KTitin) is constant for a given SL.

caused by titin-based radial force, which decreases with decreasing SL (Fig. 2) and so causes the myosin binding rate (k_{12}*KTitin) to fall, with simultaneous accumulation of RUTMon. A rise in RUTMon results in an increase of the rate parameter for the conformational change of Tm (k_{tmon}) with decreasing SL (Figs. 3B, D). The consequences of this effect will be explained further below.

The Tm conformational change is the slowest step in the activation of thin filaments, and the rate parameter k_{tmon} is very small at low [Ca^{2+}], rising linearly with an increase in [Ca^{2+}] up to the EC_{50} value for a given SL (Fig. 3). A widely accepted theory suggests that the Tm conformational change controls thin filament activation with a large movement of Tm necessary to free the myosin binding site on actin which it blocks at low [Ca^{2+}] [20]. The rate limiting step for acto-myosin interactions under isometric conditions is the ADP-release step (k_5) in the present model, as has been found in experiments in vivo [19], potentially leading to a build-up of strong Xb states (RUA_MADPPi and RUA_MADP). The model indicates maximum active tension at 2.2 μm SL with 31.3% of all RUs being in the strong Xb state, corresponding to 16.5% of available myosin heads being strongly bound. Under the assumption that only one of the two S1 heads of a myosin molecule can bind at one time, measurements suggest that only 10 to 20% of all S1 heads bind to the thin filament during maximal isometric contraction, i.e. that only 0.38 to 0.75 S1 heads are bound per RU [20]. The present model fits well with recent experimental data showing that 17–32% of myosin heads are strongly bound (by X-ray diffraction) [30] or 20–30% (by ESR) [31].

3.2. Titin's role in length-dependent activation

Concerning the LTR, a fundamental assumption is that the maximal force at a given SL is determined by the degree of overlap between thick and thin filaments which is described as "α function" (E10) in the present model. The effect on force caused by the filament overlap is the same for skeletal and cardiac muscle. To test the hypothesis that the much steeper "ascending limb" of the LTR in cardiac muscle [2,3] is due to the modulation of the lattice spacing by titin, simulation results for M1 to M4 obtained with a steady level of Ca^{2+} were compared. As shown in Fig. 4, without the effect of titin (M2), the LTR matches skeletal muscle LTR [32], but addition of the titin-based radial force (M1) to account for lattice spacing changes, that in turn changes the myosin binding rate, results in a much steeper rise of the active tension with increasing SL. M3 was used to evaluate which step, the formation of weak Xb (k_{12}) or the transition from the weak to the strong binding state (k_3), is mainly affected by interfilament spacing changes. As shown in Fig. 4, a steep LTR could only be attained if titin affects k_{12} as in M1, with the LTR for M3 being similar to M2. The LTR for M4 (Fig. 4), which uses the original mouse titin-based radial force data [8], is steeper than the LTR for M1, in which modified data were employed to account for species differences (Fig. 2). This comparison confirms that the LTR greatly depends on titin's radial force and suggests that it is highly species-dependent. M1

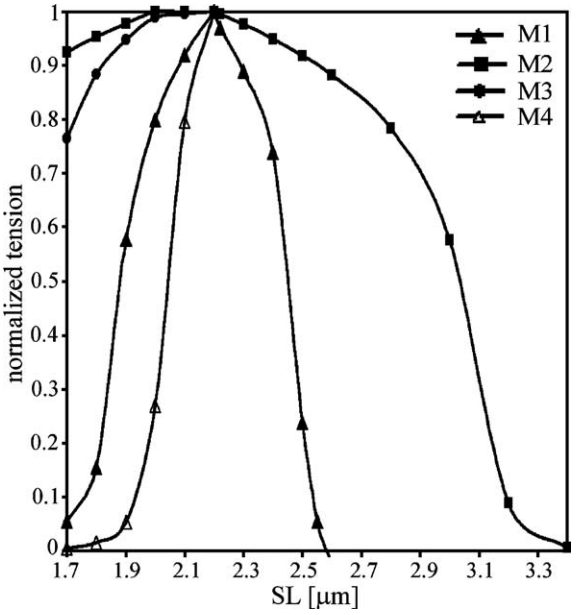

Fig. 4. Simulation results for the length–tension relationship. For M1 to M4, steady state maximum active tension which is equivalent to the tension of muscle in the titanic state was determined at constant SL for SL 1.7 to 2.2 μm, [Ca^{2+}]=1.5 μM and normalized to the maximum tension for each model. In addition, for M1 and M2, the LTR for SL>2.2 μm is shown.

and M2 were also analyzed for SL>2.2 μm. A steep tension fall results, if increased damage to titin is assumed, with rising SL above 2.2 μm (M1; E12). To sum up, simulation results support the hypothesis that titin-based radial force modulates the lattice spacing, which leads to increased formation of weak and subsequently strong Xbs with an increase of the SL in the physiological range.

3.3. Titin affects the Ca^{2+} sensitivity of myofilaments

The force–[Ca^{2+}] relationship (FCaR) indicates the level of cooperativity in filament activation measured as n_H and yields the EC_{50} value, the [Ca^{2+}] necessary for half maximum force. The following simulations were carried out for constant [Ca^{2+}] levels. Figs. 5A and B depict the FCaR for the model with titin (M1) and without titin (M2), respectively. In M2, n_H is almost constant for the SL 1.7 to 2.2 μm whereas in M1, n_H decreases from 7.95 for 2.2 μm to 4.96 for 1.9 μm and then rises to 5.84 for SL 1.7 μm (Fig. 5D). A decrease in n_H with decreasing SL was also found experimentally for skinned rat trabeculae [33] (Fig. 5D). Interestingly, this group also reported an increase in n_H for SL 1.65 μm. As shown in Fig. 5E in M1, EC_{50} greatly increases with a decrease in SL (ΔEC_{50}=1.55 μM for SL 1.7 to 2.2 μm). But the increase in EC_{50} is very small for M2 (ΔEC_{50}=0.13 μM) for the same SL range. A comparison of the ΔpCa_{50} values reveals that the change for M1 (ΔpCa_{50}=0.516) is comparable to the Kentish et al. data (ΔpCa_{50}=0.403) [33], whereas the ΔpCa_{50} values for M2 (ΔpCa_{50}=0.066) are rather comparable to the data from Dobesh et al. (ΔpCa_{50}=0.136) [34] which report a SL-

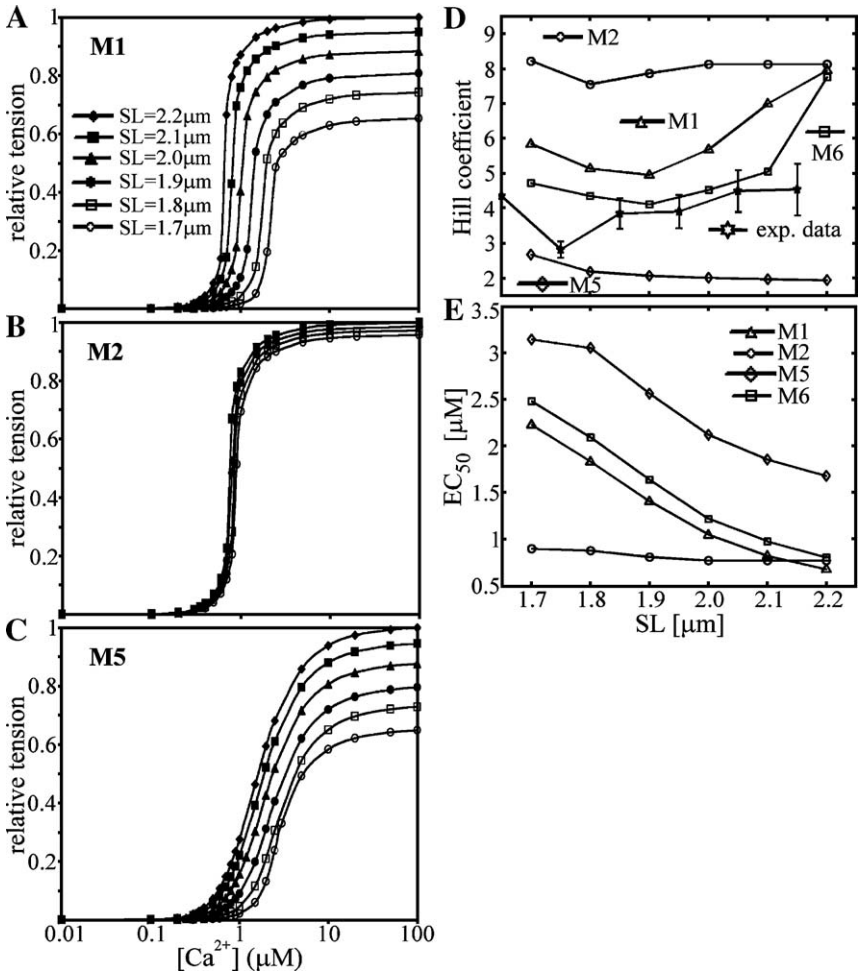

Fig. 5. Simulation results for the force–[Ca^{2+}] relationship. Panels A to C depict the steady state force normalized to maximum tension at SL=2.2 µm for each SL plotted vs. [Ca^{2+}]. Panel D compares the n_H and panel E the EC_{50} values for various SLs and different models. Experimental data shown in panel D are from skinned rat trabeculae [33].

independent n_H. Simulation results show that titin induced changes of the lattice spacing influence the myofilament Ca^{2+} sensitivity accompanied by a SL dependency of n_H.

3.4. The relationship between titin-based radial force and cooperativity

Simulation results revealed a higher cooperativity n_H at longer physiological SLs in the case titin-based radial force was taken into account (M1). Without titin (M2), the cooperativity did not change with SL and was as high as for M1 at the highest physiological SL (Fig. 5D). Thus, how does titin-based passive tension influences cooperativity? Model analysis identified the variation of the rate parameter k_{offl} through positive cooperativity caused by the number of strong Xbs as an important regulatory step. Figs. 6A and B, showing the results of numerical analysis, depict the SL-dependent change of the Xb part of k_{offl} (E4 second term) for M1 and M2, respectively. The degree of change clearly shows a coincidence of the n_H change with SL. In M1, the k_{offl} Xb part changes 15% from SL 1.7 to 2.2 µm whereas in M2 the change is only 1.4%. To further test the importance of the k_{offl} Xb part, M5 lacks the Xb-caused positive cooperativity in k_{offl} and instead the positive cooperativity caused by already activated neighboring RUs was increased ($k_{OFF}=-0.5$ compared to -0.32 in M1). However, the total cooperativity in M5 is greatly reduced (Fig. 5C) with a SL-independent $n_H \cong 2$ (Fig. 5D). EC_{50} is shifted to lower Ca^{2+} sensitivity, but an EC_{50} change ($\Delta pCa_{50}=0.272$) with SL could still be found (Fig. 5E).

The positive cooperativity caused by Xbs in k_{offl} was found to be the most important cooperativity mechanism of the whole model although other mechanisms cannot be neglected (data not shown). To validate the use of power 4.4 in E4 which implies that the influence of strong Xbs is extended to further apart RUs and not restricted to the immediate neighboring ones [21], in M6 power 4.4, a result of model fitting, was exchanged to power 2, and the resulting function fitted to the power 4.4 function through a change of k_{xboff} (from -1.37 to -2.3) to obtain a similar steepness. As shown in Fig. 5D, n_H changes with SLs, however, there is a big jump from SL 2.1 to 2.2 µm with other changes being rather small. This confirms that the exponent in the equation, hence the slope of the change with the number of Xbs, is important for the course of the SL–n_H graph.

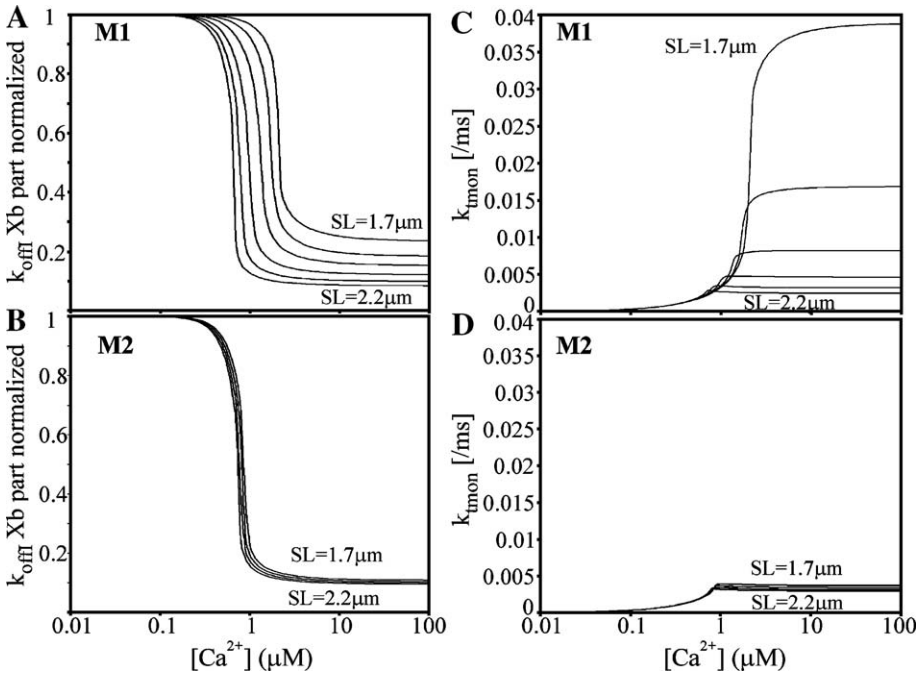

Fig. 6. SL dependency of the rate parameters k_{off} and k_{tmon}. Panels A and B illustrate the change of the part of the TnI conformational change rate parameter (k_{off}) which is due to the positive cooperativity caused by strong Xbs (second term E4) with [Ca^{2+}] for various SLs and panels C and D the change of the Tm conformational change rate parameter k_{tmon} (E7) for M1 and M2, respectively. These simulations were performed with the numerical analysis program.

Interestingly, for smaller SLs n_H starts rising again in M1 (Fig. 5D) as was reported experimentally [33]. This is caused by a change of the rate parameter k_{tmon} with SLs in M1 (Fig. 6C) which is negligible in M2 (Fig. 6D). This may be explained as follows: with decreasing SLs, the rate parameter k_{12} decreases due to lattice spacing changes caused by titin-based radial tension which causes RUTMon to rise (Fig. 3). A part of the positive cooperativity affecting k_{tmon} is due to the concentration of RUTMon (E7), hence the rise of k_{tmon} with a rise in RUTMon.

3.5. Analysis of isosarcometric twitch contractions

To get a Ca^{2+} transient for the simulation of twitch contractions, M1 was inserted into the Kyoto Model (KM) [22] which had the previous contraction model removed (labeled M1(KM)). The KM is a comprehensive ventricular myocyte model that combines excitation with contraction and includes the SR and several ion pumps and channels. Major cellular components that contribute to the Ca^{2+} transient are the L-type Ca^{2+} channel, the ryanodine receptor, the SR Ca^{2+} pump, and the Na^+/Ca^{2+} exchanger. In addition, calmodulin is used as an intracellular Ca^{2+} buffer. The KM and the contraction model are only connected through the intracellular [Ca^{2+}]. The present model could be inserted into any model which produces a Ca^{2+} transient. The KM was chosen because it gives a Ca^{2+} transient adjusted to guinea pig data at 2.5 Hz stimulation frequency. However, since the Ca^{2+} transient was adjusted to the previously in the KM included contraction model [22], the peak [Ca^{2+}] obtained with M1 in the KM is higher.

Fig. 7A depicts twitch contractions for various SLs and the Ca^{2+} transient produced by the KM. As expected with an increase in SL, active tension rises. The rate of force development is approximately proportional to peak force, i.e. the time to reach 90% peak force (TTP90) is about the same for all SLs (Fig. 7B, C; ΔTTP90 = 8.99 ms for SL 1.7–2.2 μm). Experimental data obtained from rat trabeculae showed that TTP90 is almost constant for all SLs under same conditions [35]. However, a remarkable variation of the time required for 50% relaxation (R50; measured from the time of peak tension) with SL was reported with ΔR50 strongly dependent on extracellular [Ca^{2+}] [35]. An increase in SL also caused an increase in R50 in simulations with M1 (Fig. 7D; ΔR50 = 41.1 ms for SL 1.7–2.2 μm). An indirect correlation of relaxation times with tension was reported for rat trabeculae which was independent of temperature [36]. Simulation results for M1 and M5, which both include titin and show an EC_{50} change with SL, reveal the same nonlinear relationship between peak tension and R50 (Fig. 7D). However, M2 which lacks titin shows a linear relationship between tension and R50, i.e. the increase of the active tension (F_b) with a rise in SL is parallel to the increase of R50 with SL. These data suggest that at a constant stimulation frequency SL-dependent relaxation times are influenced by the length-dependent Ca^{2+} sensitivity mechanism and depend on titin and not only on peak tension.

M1 twitch contraction data are comparable to data from guinea pig intact ventricular myocytes recorded at slack length (1.88 μm; 35 °C; 3.6 mM Ca; 1 Hz) with peak force 5.3 ± 2.6 mN/mm^2 vs. 3.8 mN/mm^2 for M1, time to peak tension 93 ± 21 ms vs. 106 ms for M1 and time to 90% relaxation 235 ± 63 ms vs. 233 ms for M1 at 1.88 μm SL [37]. Since the KM is adjusted to 2.5 Hz stimulation frequency, relaxation in M1 might be a little slow. In this model, negative

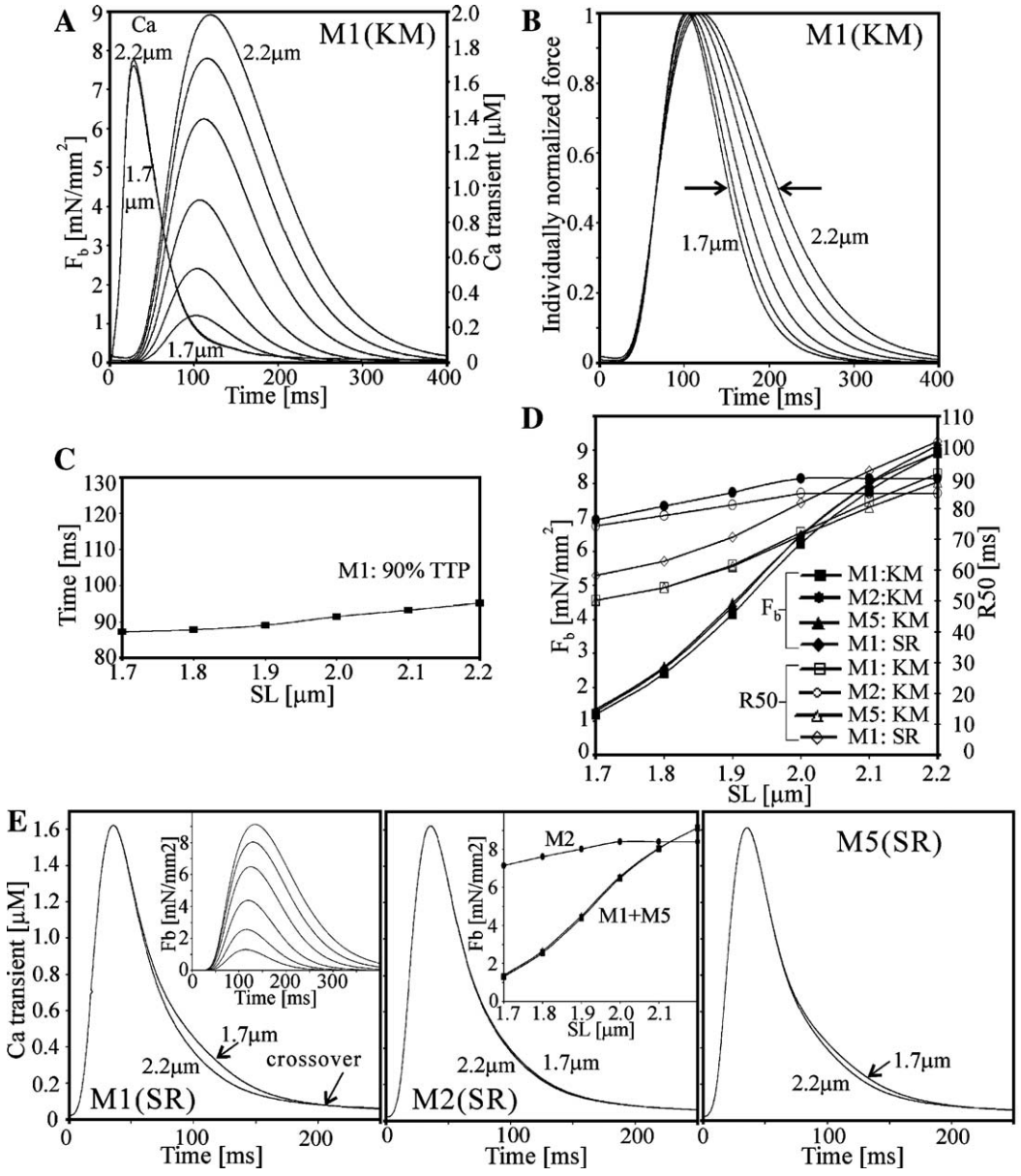

Fig. 7. Simulation results for twitch contractions and analysis of relaxation. Panel A shows the active tension for M1 for different SLs (1.7, 1.8, 1.9, 2.0, 2.1 and 2.2 µm) and the buffered Ca^{2+} transient for SL 1.7 and 2.2 µm obtained by the KM [22] which is adjusted to 2.5 Hz stimulation frequency. At panel B, active tension of M1 was normalized to the peak twitch tension level for each SL. The arrows indicate the 50% relaxation time. Stimulation occurred at 0 ms. In panel C, 90% TTP data for M1 have been plotted against SLs. Panel D shows the SL-dependent relationship of peak tension and R50 for M1(KM), M2(KM), M5(KM) and M1(SR). Panel E shows the nonbuffered Ca^{2+} transients for SL 1.7 and 2.2 µm for twitch contraction from M1, M2 and M5 obtained by adding a simple SR to the contraction model as described in [28] (E8 and E9 in [28]; Q_m was changed to 0.00095 mM/ms and K_p to 0.0002 mM/ms). The insert in the left panel depicts the time course for M1(SR) twitch contractions at different SLs. The insert in the middle panel displays the SL-dependency of the peak tension for M1(SR), M2(SR) and M5(SR).

cooperativity acts to balance the tension rise rather than speeding up relaxation, i.e. peak tension is reduced and therefore relaxation starts earlier (data not shown). This effect is greater the larger the SL in the physiological range. Late relaxation is not effected. Further mechanisms to regulate relaxation, such as hormonal regulation like β-stimulation need to be added to the model in the future.

Experimental results from ferret and rat cardiac muscles injected with Ca^{2+} sensitive fluorescent dyes showed that the peak $[Ca^{2+}]$ of the Ca^{2+} transient does not significantly change with SL given a constant stimulation frequency [38,39], although a change of the peak $[Ca^{2+}]$ with SL variation was detected with some experimental procedures [40]. Furthermore, all groups reported a faster relaxation of the Ca^{2+} transient with an increase in SL, whereas the tension decay was prolonged [38–40], and it was suggested that the affinity of TnC for Ca^{2+} is influenced by the number of strong Xbs. In accordance to these experimental data, the peak $[Ca^{2+}]$ of the Ca^{2+} transient did not change notably with SL in simulations using the KM with M1 (Fig. 7A). However, no change of the Ca^{2+} transient relaxation was found for different SLs. This might be caused by a too-strong Ca^{2+} buffer in the KM where a constant intracellular

calmodulin concentration $[CaM]_i$ of 50 μM is applied [22]. In contrast, the total $[CaM]_i$ was estimated to be about 6 μM in cardiac myocytes [41]. To check whether the simulation results are indeed due to a problem with the Ca^{2+} buffer, a simple nonbuffered SR component [28] was added to the isolated contraction model (labeled SR). The Ca^{2+} transient thus predicted is controlled by the inflow (Q_{pump}, E8 of [28]) and outflow (Q_{rel}, E9 of [28]) of Ca^{2+} from the SR and has a shape different from that of the KM Ca^{2+} transient. Fig. 7E (left panel) shows the Ca^{2+} transient for SL 1.7 and 2.2 μm for M1(SR). The peak $[Ca^{2+}]$ of the Ca^{2+} transient is the same for both SLs but relaxation rate changes with SL, as was also found experimentally [38–40]. For 2.2 μm SL, the Ca^{2+} transient relaxation is initially faster than for 1.7 μm, but the late relaxation is slower. Interestingly, such a crossover of the Ca^{2+} transients obtained at two different SLs has been reported from in vivo experiments [38]. Due to the different shape of this Ca^{2+} transient compared to the one obtained from the KM, tension relaxation is prolonged (Fig. 7E insert left panel), but the relationship between peak tension and R50 is nonlinear, regardless of the Ca^{2+} transient utilized (Fig. 7D), i.e. a change of the Ca^{2+} transient relaxation with a change in SL has no effect on tension relaxation. To analyze the cause of the change in Ca^{2+} transient relaxation with SL variation, the influences of M1 (SR), M2 (SR) and M5 (SR) on the Ca^{2+} transient were compared (Fig. 7E). No change in the Ca^{2+} transient was found for the contraction model that lacks titin (M2). If the connection of strong Xbs to the rate parameter k_{offl} is missing, as in M5, there is still a change in Ca^{2+} transient relaxation, but the effect is smaller, although M1 and M5 exhibit the same SL-dependency of peak tension (Fig. 7E insert middle panel). In conclusion, simulation results demonstrate that titin is essential to reproduce experimental findings but the positive cooperativity caused by strong Xbs which influences the rate parameter k_{offl} is necessary to further enhance Ca^{2+} transient relaxation. These findings support the hypothesis stated by experimentalists [38–40], that strong Xbs are involved in the change of the Ca^{2+} transient relaxation with SL.

4. Discussion

The major achievement of this work is the elucidation of a working hypothesis of Frank–Starling's law using a cardiac contraction model that combines recent experimental data on cooperativity in filament activation and on interfilament lattice spacing modulation through titin-based passive tension. This is to our knowledge the first time that the giant sarcomeric protein titin was included in a contraction model and that a mechanism of Frank–Starling was tested and analyzed by simulation.

4.1. A new generation of cardiac muscle contraction models

Starting with Huxley [42], many cardiac muscle contraction models were developed, ranging from relatively simple models [23,28,43,44] to mathematically highly complex models [45]. However, the majority of these models include nonexistent lumped states with a missing link to molecular mechanisms. A lack in understanding fundamental mechanisms underlying contraction was stated as the reason for the missing breakthrough in modeling contraction [46]. However, in the last few years, a great experimental effort shed light on some important regulatory mechanisms of cardiac muscle such as the involvement of titin-based passive tension in the active tension development [9] and of TnI in the Ca^{2+} activation of striated muscle [15]. These experimental results were included in the present model, which is based on the molecular level and consists of 7 different activation and/or conformational states of the molecular RU of which actin filaments are composed. All these states of the RU are connected, in contrast to published models in which states are split into separate parts [16,44]. This model uses experimental data for titin-based radial force to alter the myosin binding rate with SL change. The conformational change of TnI is subject to cooperativity caused by Xbs. It is merely the combination of titin and the TnI conformational change which makes the present model quite distinct from all published models. Here it is shown that the model well reproduces major isometric contraction characteristics, such as the twitch contraction time course, the LTR and the FCaR including high cooperativity.

4.2. Modeling SL-dependent Ca^{2+} sensitivity

For skeletal muscle, the shape of the LTR was attributed to the change of the acto-myosin filament overlap with SLs. The cause of the steep LTR in cardiac muscle has still not been completely solved, but recent experimental results give evidence that the radial force produced by the giant elastic protein titin may reduce the interfilament lattice spacing upon increased SL which leads to a change of the active tension [5,8,9]. This was confirmed with the present model (M1), in which the myosin binding rate changes proportionally to the radial force produced by titin, according to slightly modified mouse experimental data (Fig. 2). Simulation results indicate that titin alone would be sufficient to account for a steep LTR and an increase in the Ca^{2+} sensitivity with an increase in SL (Figs. 4 and 5A). In M1, a decrease of SL from 2.2 to 2.0 μm results in a 20% decrease of the maximum active tension, matching experimental results [47]. In contrast, results for M2, which excludes titin, show a LTR as found for skeletal muscle [32], and the EC_{50} change with SL is negligible (Figs. 4 and 5B).

The model predicts a direct relationship between titin-based radial force and the steepness of the LTR. A change of the ascending limb of the titin function (E11) results in a change of the LTR, as confirmed by M4, which includes the original mouse data with a higher titin-based passive tension (Fig. 2, E29), leading to a steeper LTR (Fig. 4). Since titin-based radial force is highly tissue and species-dependent [1,24], this also applies to the LTR as reported recently. In bovine ventricular muscle, which exhibits a higher titin-based passive tension than bovine atrial muscle, a stronger SL dependency of maximal active tension was found [5].

Among published contraction models [23,28,44], this present model is unique in explaining the SL dependency in Ca^{2+} sensitivity since the SL is only included in the myosin binding step and the Ca^{2+} binding rate is constant [16]. A

change of the TnC affinity for Ca^{2+} requires a TnC conformational change induced by a change in the conformation of the Tn complex, such as phosphorylation of TnI by protein kinase A (PKA) which was shown to alter the Ca^{2+} sensitivity of TnC [48]. Since SL-dependent Ca^{2+} sensitivity can also be seen in isolated and skinned cardiac muscle [8], where kinases may no longer be present, a conformational change of the Tn complex cannot be the fundamental mechanism. Furthermore, neither an overexpression of skeletal TnC in cardiac muscle [49] nor a change in the affinity of cardiac TnC for Ca^{2+} with the Ca^{2+} sensitizer pimobendan [12] altered the length-dependent activation [5]. In conclusion, the present model supports the hypothesis that titin's effect on the lattice spacing is essential for the Frank–Starling law with additional mechanisms, such as phosphorylation by PKA, probably necessary for fine tuning of regulatory steps. Moreover, PKA-mediated phosphorylation of titin was reported to increase its compliance [50].

4.3. Enhanced cooperativity at longer SLs

In a cell, almost all reactions are strictly regulated, and so rate parameters change dynamically. To achieve a high cooperativity in a contraction model, a dynamic feedback of state concentrations with an active change of some rate parameters is essential. A dynamic change of the following three rate parameters was found important for the present model (Fig. 1): (1) k_{offI}, the rate parameter for the conformational change of TnI to the inactive form, (2) k_{tmon}, the rate parameter for the Tm conformational change to the "on" conformation and (3) k_3, the rate parameter for the force generating step. A change of the Xb dissociation rate (k_{-3}) was tested [16], but found to be negligible. Simplified equations with a similar structure to the nearest-neighboring statistics [21], i.e. power 2 terms, were employed. Using power 2 implies that only the two immediate neighboring RUs are affected by an activated RU [15,21]. However, in the case of positive cooperativity caused by strong Xbs which effects k_{offI}, the most important cooperativity mechanism in the model, an exponent greater than 2 was required. This cooperativity played a sensitive role in model adjustment. A variation in the exponent or parameter values easily resulted in an unrealistic SL dependency of n_H or unacceptable n_H values (M6, Fig. 5D). Indeed, it was suggested that the actin–myosin interaction and its effect on Ca^{2+} sensitivity are highly sensitive to changes in proximity and that the relationship between interfilament spacing and myofilament Ca^{2+} sensitivity is nonlinear [6]. In addition, the fact that an exponent greater than 2 was essential demonstrates that not all cooperativity is mediated by the same mechanism and the influence strength of an activated RU to the neighboring RUs may differ. Strong Xbs may have a stronger influence in the inhibition of the TnI actin re-association affecting further RUs as well. In conclusion, the present model confirms the importance of the TnI conformational change as a potential regulatory switch [15].

A controversial subject among experimentalist is the SL dependency of n_H with some groups reporting an increase of n_H with an increase in SL [9,33], and others stating that n_H is SL-independent [34]. Presumably, the experimental determination of n_H is strongly dependent on experimental conditions such as the $[Mg^{2+}]$. Here modeling can give an unambiguous answer. For the model without the titin function (M2), n_H is high and independent of the SL. However, adding the titin function to the model (M1) results in a strong SL dependency of n_H with n_H decreasing from SL 2.2 to 1.9 μm and rising again for smaller SLs, matching experimental data from skinned rat trabeculae [33] (Fig. 5D). A small increase of n_H at shorter SL was also found in ferret intact muscle [51]. Simulation results indicate that the SL dependency of n_H is caused by titin-based radial force affecting the myosin binding rate and confirm the hypothesis that titin-based passive tension enhances cooperative activation [9]. Some experimental evidence for a titin influence on the SL dependency of n_H was reported. Controlled trypsin treatment of cardiac muscle which specifically degrades about 40% of the I-band region of titin led to a decrease of titin-based passive tension and resulted in an attenuation of the SL-dependent Ca^{2+} sensitivity [9]. In trypsin treated muscle, Δn_H (0.44) and ΔEC_{50} (0.11) were smaller than for control muscle specimens ($\Delta n_H = 0.79$; $\Delta EC_{50} = 0.16$) for the SL range 1.9 to 2.25 μm, i.e. a reduced titin effect diminishes the SL dependency of n_H and EC_{50}. An increase of n_H at smaller SLs may be explained in the present model through an increase of the rate parameter k_{tmon} due to a rise in positive cooperativity with decreasing SL (Fig. 6C). Overall a high cooperativity ($n_H > 7$) comparable to in vivo experimental data [34,52,53] was achieved (Fig. 5D).

4.4. Titin's influence on myofilament relaxation

Proper relaxation after contraction is essential for efficient filling of the heart. The mechanisms underlying relaxation of myofilaments, characterized by R50, the time required for 50% relaxation from peak tension, are even less well understood than those governing activation. R50 is controlled by the Ca^{2+} transient and by properties of the myofilaments, such as changes occurring after SL modulation and the Ca^{2+} affinity of TnC [35,54]. Since no significant change of the Ca^{2+} transient magnitude with SL could be detected in most experiments [38–40] or in the present model (Figs. 7A, E), the dependency of relaxation on length is presumably a myofilament characteristic. As found by in vivo experiments [35,36], at a constant stimulation frequency, an increase in SL resulted in an increase of relaxation times for all model variants tested (Fig. 7D). A change in the Ca^{2+} transient relaxation with SL did not affect tension relaxation, as is shown in Fig. 7D (M1(KM) and M1 (SR)). The relationship between the increase in peak tension and the increase in R50 is nonlinear for M1. However, for M2, the model which lacks titin, this relationship becomes linear (Fig. 7D). Results for M5, which includes titin but lacks the positive cooperativity caused by Xbs in k_{offI}, are similar to M1. This suggests that the tension–R50 relationship is influenced by titin-based modulation of lattice spacing causing the EC_{50} change with SL, but is not effected by the cooperativity which is low in M5 (Fig. 5D). A recent simulation study focusing on

myocyte relaxation analyzed the effect of SL on R50 [54]. It was reported that the SL-tension dependence had a minimal effect on R50 whereas the length-dependent Ca^{2+} sensitivity had a significant effect. In that study, a contraction model which lacked titin and a Frank–Starling mechanism was used, and it was assumed that n_H is SL-independent. Furthermore, that study suggested that either the tension dependence of Ca^{2+} binding to TnC or that bound Xbs which inhibit Tm from returning to the "off" state is responsible for the increase in relaxation time with SL [54]. The present study confirmed that the length-dependent Ca^{2+} sensitivity influences relaxation, but this is due to lattice spacing modulation caused by titin and seems to be independent of cooperativity and of an affinity change of TnC for Ca^{2+}.

4.5. A potential Frank–Starling mechanism

Despite a huge experimental effort to elucidate the complex mechanisms behind the heart's fundamental Frank–Starling law there is still a lack of understanding [4,5]. An analysis of the present model indicates that two mechanisms, (1) lattice spacing modulation through titin-based radial force effecting the myosin binding rate and (2) the positive cooperativity caused by strong Xbs regulating the TnI conformational change, are both important for length-dependent activation [9,15], and must act synergistically to explain the Frank–Starling effect (M1). Omitting either mechanism results in a failure: M2, which lacks titin, gives a LTR similar to skeletal muscle (Fig. 4) and shows no SL dependency of n_H and EC_{50} (Figs. 5B, D, E). M5, where the positive cooperativity caused by Xbs has been omitted in k_{offl}, shows a very low cooperativity which is SL-independent (Figs. 5C, D). The cooperation of both mechanisms explains how titin might affect Ca^{2+} sensitivity: a change of the interfilament lattice-spacing through titin-based SL-dependent passive tension causes SL-dependent alteration of the myosin binding rate (k_{12}), which in turn affects the number of strong Xbs. The amount of strong Xbs regulates the TnI conformational change (k_{offl}). The higher the Xb concentration, the more TnI is prevented from taking the "off" conformation. Hence, the Xb concentration which is determined through titin's passive tension influences the Ca^{2+} sensitivity of the Tn complex.

The following experimental findings support this proposed mechanism: First, titin-based radial force modulates the interfilament lattice spacing, and the SL dependency of n_H was diminished in muscles where titin was partially degraded by trypsin [9]. Furthermore, SL dependency of maximum active tension was more pronounced, i.e. a steeper LTR, in muscles with greater titin-based passive tension [5]. Next, based on in vitro experimental findings, a two-step model for Ca^{2+} activation of thin filaments, involving TnC and TnI with strong Xb-induced inhibition of the TnI conformational change to the "off" state, was proposed [15]. Several experimental data confirmed that strong Xbs exhibit positive cooperativity [11–14] (see Introduction). In addition, lowering the MgATP concentration to a level at which actin and myosin bind tightly causes an increase of developed tension in a Ca^{2+} free solution [55].

4.6. Model limitations

Every model exhibits limitations which are due to simplifications and to unsolved mechanisms. Here discussion is focussed on the diversity of mechanisms. Several potential cooperativity mechanisms in thin filament activation have been reported some supported by experimental evidence [20]. In this model, special attention was given to the TnI conformational change, where in vitro experimental results [15] show that this may be an important regulatory switch in the activation of actin filaments. The importance of this step may be overestimated in the present model with the Tm conformational change being somewhat neglected. Tm exists in this model only in the "on" (RUTMon) or "off" (RUTCaon) states, but this step is the rate limiting step of the filament activation part (Section 3.1). Experimental evidence [20] suggests that Tm may be present in three different states: Upon binding of Ca^{2+} to TnC, Tm was found to move $\sim 25°$ around on the surface of the actin filament, changing from the "blocking" to the "closed" state, thereby exposing several myosin binding sites and allowing weak acto-myosin interactions. Addition of S1 heads resulted in a second movement by Tm of $\sim 10°$ to the so-called "open" state, which allows strong Xb formation. This latter effect was only seen with more than one S1 head bound per RU [20]. In the present model, it was assumed that only one strong Xb can be formed per RU, and this mechanism was not taken into account. This is justified since it is still not proven whether Tm or TnI binding to actin prevents interaction in the resting state [56]. Furthermore, it has been suggested [56] that Tm facilitates the transmission of the effects resulting from the TnI conformational change to other RUs, rather than having a "blocking" role. This suggestion was applied in this model through positive cooperativity exhibited by RUTCaon and RUTMon which enhance the rate parameters k_{tmon} and k_3. In addition, strong Xbs affect k_{tmon} through negative cooperativity, i.e. slowing down rather than enhancing filament activation, as would occur in the case of a three-state Tm activation.

Another unsolved question is the order of events in the Xb cycle [20]. In this model, the force generation step precedes P_i release, based on experimental findings by Sleep et al. [19]. But it has also been suggested that force generation and P_i release occur in the same step [20,57]. Moreover, two steps of the Xb cycle, namely binding of ATP to acto-myosin to dissociate myosin from actin, and the subsequent release of ATP from the detached myosin, were neglected, and myosin dissociation was lumped into the ADP release step.

Our work confirms that simulation is a powerful tool to study complex biological mechanisms, combining various experimental results in one model. The Frank–Starling mechanism found in the present cardiac contraction model is probably one of many existing mechanisms, and validation through further experiments is needed. However, to our knowledge, this is the first time a complete Frank–Starling mechanism has been suggested and analyzed, and this model seems well suited in studying the SL-dependent Ca^{2+}

activation since it includes titin, a protein which is increasingly being found important; for example, a change of the titin isoform ratio was detected in diseased human hearts [7].

Acknowledgments

The authors wish to thank Prof. Akinori Noma for discussion and Piers Vigers for improving the English of this paper. This study was supported by the Leading Project for Biosimulation from the Ministry of Education, Culture, Sports, Science and Technology of Japan.

References

[1] Wu Y, Cazorla O, Labeit D, Labeit S, Granzier H. Changes in titin and collagen underlie diastolic stiffness diversity of cardiac muscle. J Mol Cell Cardiol 2000;32:2151–62.
[2] Allen DG, Jewell BR, Murray JW. The contribution of activation processes to the length–tension relation of cardiac muscle. Nature 1974;248:606–7.
[3] Sonnenblick EH, Skelton CL. Reconsideration of the ultrastructural basis of cardiac length–tension relations. Circ Res 1974;35:517–26.
[4] Moss RL, Fitzsimons DP. Frank–Starling relationship: long on importance, short on mechanism. Circ Res 2002;90:11–3.
[5] Fukuda N, Granzier HL. Titin/connectin-based modulation of the Frank–Starling mechanism of the heart. J Muscle Res Cell Motil in press.
[6] Fuchs F, Martyn DA. Length-dependent Ca^{2+} activation in cardiac muscle: some remaining questions. J Muscle Res Cell Motil 2005;26:199–212.
[7] Granzier HL, Labeit S. The giant protein titin: a major player in myocardial mechanics, signaling, and disease. Circ Res 2004;94:284–95.
[8] Cazorla O, Wu Y, Irving TC, Granzier H. Titin-based modulation of calcium sensitivity of active tension in mouse skinned cardiac myocytes. Circ Res 2001;88:1028–35.
[9] Fukuda N, Wu Y, Farman G, Irving TC, Granzier H. Titin-based modulation of active tension and interfilament lattice spacing in skinned rat cardiac muscle. Pflugers Arch 2005;449:449–57.
[10] Neagoe C, Opitz CA, Makarenko I, Linke WA. Gigantic variety: expression patterns of titin isoforms in striated muscles and consequences for myofibrillar passive stiffness. J Muscle Res Cell Motil 2003;24:175–89.
[11] Fitzsimons DP, Moss RL. Strong binding of myosin modulates length-dependent Ca^{2+} activation of rat ventricular myocytes. Circ Res 1998;83:602–7.
[12] Fukuda N, Kajiwara H, Ishiwata S, Kurihara S. Effects of MgADP on length dependence of tension generation in skinned rat cardiac muscle. Circ Res 2000;86:E1–6.
[13] Adhikari BB, Regnier M, Rivera AJ, Kreutziger KL, Martyn DA. Cardiac length dependence of force and force redevelopment kinetics with altered cross-bridge cycling. Biophys J 2004;87:1784–94.
[14] Fukuda N, O-Uchi J, Sasaki D, Kajiwara H, Ishiwata S, Kurihara S. Acidosis or inorganic phosphate enhances the length dependence of tension in rat skinned cardiac muscle. J Physiol 2001;536:153–60.
[15] Robinson JM, Dong WJ, Xing J, Cheung HC. Switching of troponin I: Ca^{2+} and myosin-induced activation of heart muscle. J Mol Biol 2004;340:295–305.
[16] Schneider NS, Shimayoshi T, Amano A, Matsuda T, Noma A. Including titin in a simple muscle contraction model suitable for a myocardial cell model. In: Hozman J, Kneppo P, editors. EMBEC'05. IFMBE Proceedings of the 3rd European Medical and Biological Engineering Conference; 2005 Nov 20–25; Prague, Czech Republic, vol. 11. Prague, Czech Republic: International Federation for Medical & Biological Engineering; 2005. p. 2642–7. [CD-ROM].
[17] Solaro RJ, Rarick HM. Troponin and tropomyosin: proteins that switch on and tune in the activity of cardiac myofilaments. Circ Res 1998;83:471–80.
[18] Bers DM. Excitation-contraction coupling and cardiac contractile force. 2nd ed. Dordrecht: Kluwer Academic Publishers; 2001.
[19] Sleep J, Irving M, Burton K. The ATP hydrolysis and phosphate release steps control the time course of force development in rabbit skeletal muscle. J Physiol 2005;563:671–87.
[20] Gordon AM, Homsher E, Regnier M. Regulation of contraction in striated muscle. Physiol Rev 2000;80:853–924.
[21] Robinson JM, Wang Y, Kerrick WG, Kawai R, Cheung HC. Activation of striated muscle: nearest-neighbor regulatory-unit and cross-bridge influence on myofilament kinetics. J Mol Biol 2002;322:1065–88.
[22] Matsuoka S, Sarai N, Kuratomi S, Ono K, Noma A. Role of individual ionic current systems in ventricular cells hypothesized by a model study. Jpn J Physiol 2003;3:105–23.
[23] Rice JJ, Raimond LW, William CH. Comparison of putative cooperative mechanisms in cardiac muscle: length dependence and dynamic responses. Am J Physiol 1999;276:H1734–54.
[24] Cazorla O, Freiburg A, Helmes M, Centner T, McNabb M, Wu Y, et al. Differential expression of cardiac titin isoforms and modulation of cellular stiffness. Circ Res 2000;86:59–67.
[25] Rouslin W. The mitochondrial adenosine 5′-triphosphatase in slow and fast heart rate hearts. Am J Physiol 1987;252:H622–7.
[26] Li H, Linke WA, Oberhauser AF, Carrion-Vazquez M, Kerkvliet JG, Lu H, et al. Reverse engineering of the giant muscle protein titin. Nature 2002;418:998–1002.
[27] Weiwad WK, Linke WA, Wussling MH. Sarcomere length–tension relationship of rat cardiac myocytes at lengths greater than optimum. J Mol Cell Cardiol 2000;32:247–59.
[28] Negroni JA, Lascano EC. A cardiac muscle model relating sarcomere dynamics to calcium kinetics. J Mol Cell Cardiol 1996;28:915–29.
[29] Sarai N, Matsuoka S, Noma A. simBio: a Java package for the development of detailed cell models. Prog Biophys Mol Biol 2006;90:360–77.
[30] Bershitsky SY, Tsaturyan AK, Bershitskaya ON, Mashanov GI, Brown P, Burns R, et al. Muscle force is generated by myosin heads stereospecifically attached to actin. Nature 1997;388:186–90.
[31] Ostap EM, Barnett VA, Thomas DD. Resolution of three structural states of spin-labeled myosin in contracting muscle. Biophys J 1995;69:177–88.
[32] Gordon AM, Huxley AF, Julian FJ. The variation in isometric tension with sarcomere length in vertebrate muscle fibres. J Physiol 1966;184:170–92.
[33] Kentish JC, ter Keurs HE, Ricciardi L, Bucx JJ, Noble MI. Comparison between the sarcomere length–force relations of intact and skinned trabeculae from rat right ventricle. Influence of calcium concentrations on these relations. Circ Res 1986;58:755–68.
[34] Dobesch PD, Konhilas JP, de Tombe PP. Cooperative activation in cardiac muscle: impact of sarcomere length. Am J Physiol 2002;282:H1055–62.
[35] Janssen PM, Hunter WC. Force, not sarcomere length, correlates with prolongation of isosarcometric contraction. Am J Physiol 1995;269:H676–85.
[36] Janssen PM, Stull LB, Marban E. Myofilament properties comprise the rate-limiting step for cardiac relaxation at body temperature in the rat. Am J Physiol 2002;282:H499–507.
[37] Shepherd N, Vornanen M, Isenberg G. Force measurements from voltage-clamped guinea pig ventricular myocytes. Am J Physiol 1990;258:H452–9.
[38] Backx PH, TerKeurs HE. Fluorescent properties of rat cardiac trabeculae microinjected with fura-2 salt. Am J Physiol 1993;264:H1098–110.
[39] Komukai K, Kurihara S. Effect of developed tension on the time courses of Ca^{2+} transients and tension in twitch contraction in ferret myocardium. Cardiovasc Res 1996;32:384–90.
[40] Allen DG, Kurihara S. The effects of muscle length on intracellular calcium transients in mammalian cardiac muscle. J Physiol 1982;327:79–94.
[41] Maier LS, Bers DM. Calcium, calmodulin, and calcium–calmodulin kinase II: heartbeat to heartbeat and beyond. J Mol Cell Cardiol 2002;34:919–39.
[42] Huxley AF. Muscle structure and theories of contraction. Prog Biophys Biophys Chem 1957;7:255–318.
[43] Landesberg A, Sideman S. Mechanical regulation of cardiac muscle by coupling calcium kinetics with cross-bridge cycling: a dynamic model. Am J Physiol 1994;267:H779–95.
[44] Sachse FB, Glänzel KG, Seemann G. Modeling of protein interactions

involved in cardiac tension development. Int J Bifurc Chaos 2003; 13:3561–78.
[45] Campbell KB, Razumova MV, Kirkpatrick RD, Slinker BK. Nonlinear myofilament regulatory processes affect frequency-dependent muscle fiber stiffness. Biophys J 2001;81:2278–96.
[46] Rice JJ, de Tombe PP. Approaches to modeling crossbridges and calcium-dependent activation in cardiac muscle. Prog Biophys Mol Biol 2004; 85:179–95.
[47] Fuchs F. Mechanical modulation of the Ca^{2+} regulatory protein complex in cardiac muscle. News Physiol Sci 1995;10:6–12.
[48] Dong WJ, Wang CK, Gordon AM, Rosenfeld SS, Cheung HC. A kinetic model for the binding of Ca^{2+} to the regulatory site of troponin from cardiac muscle. J Biol Chem 1997;272:19229–35.
[49] McDonald KS, Field LJ, Parmacek MS, Soonpaa M, Leiden JM, Moss RL. Length dependence of Ca^{2+} sensitivity of tension in mouse cardiac myocytes expressing skeletal troponin C. J Physiol 1995;483:131–9.
[50] Fukuda N, Wu Y, Nair P, Granzier HL. Phosphorylation of titin modulates passive stiffness of cardiac muscle in a titin isoform-dependent manner. J Gen Physiol 2005;125:257–71.
[51] Komukai K, Kurihara S. Length dependence of Ca^{2+}–tension relationship in aequorin-injected ferret papillary muscles. Am J Physiol 1997;273: H1068–74.
[52] Yue DT, Marban E, Wier WG. Relationship between force and intracellular $[Ca^{2+}]$ in tetanized mammalian heart muscle. J Gen Physiol 1986;87:223–42.
[53] Gao WD, Backx PH, Azan-Backx M, Marban E. Myofilament Ca^{2+} sensitivity in intact versus skinned rat ventricular muscle. Circ Res 1994;74:408–15.
[54] Niederer SA, Hunter PJ, Smith NP. A quantitative analysis of cardiac myocyte relaxation: a simulation study. Biophys J 2006;90:1697–722.
[55] Fuchs F, Smith SH. Calcium, cross-bridges, and the Frank–Starling relationship. News Physiol Sci 2001;16:5–10.
[56] Perry SV. What is the role of tropomyosin in the regulation of muscle contraction? J Muscle Res Cell Motil 2003;24:593–6.
[57] Gordon AM, Regnier M, Homsher E. Skeletal and cardiac muscle contractile activation: tropomyosin “rocks and rolls”. News Physiol Sci 2001;16:49–55.
[58] Lan G, Sun SX. Dynamics of myosin-driven skeletal muscle contraction: I. Steady-state force generation. Biophys J 2005;88:4107–17.